Ring-Shear Tests on Sliding Surface Liquefaction Behavior of Sandy Soils

WANG Fawu* and Kyoji SASSA

*Graduate School of Science, Kyoto University, Japan

Synopsis

To study the mechanism of rapid landslide, especially, the factors affecting high-mobility, three series of ring shear tests (drained speed-controlled test, undrained speed-controlled test and undrained cyclic-loading test) were conducted by ring-shear system. The employed samples were Toyoura standard sand, silica sand and Osaka group coarse, sandy soil. Excess pore pressure ratio, expressed as excess pore pressure with respect to the initial effective normal stress, was used as an evaluation index for the degree of mobility. The test results showed that, in the soil susceptible to grain crushing in drained tests, the pore pressure generate easily both in undrained speed-controlled test and undrained cyclic-loading tests. Parametric studies, involving initial stress state, initial relative density, and frequency of cyclic-loading were also performed.

Keywords: sliding surface liquefaction; ring-shear tests; landslide; cyclic-loading; excess pore pressure ratio; high-mobility

1. Introduction

Landslide is a common geo-hazard in mountainous area with the progress of regional development due to population growth and urbanization, especially in high seismic area. Those with high-mobility often cause great damage and loss to the society (Sassa et al., 1996; Sassa et al., 1997). Investigation on the factors that cause high-mobility is very important to disaster mitigation. Based on triaxial compression tests, many achievements have been accomplished. The 'pontaneous liquefaction' phenomenon was considered to be the main cause of slope failures likely to occur in saturated deposits of fine silty sands (Terzaghi et al., 1948; Seed and Lee, 1966; Castro, 1969; Ishihara, 1993). Recently, a concept of 'Sliding Surface Liquefaction' was proposed by Sassa et al. (Sassa, 1996; Sassa et al., 1996), in studies of some landslides triggered by the 1995.1.17 Hyogoken-Nanbu earthquake through the undrained ring-shear tests. They explained the difference between (mass) liquefaction and sliding surface liquefaction as follows: "(Mass) Liquefaction is normally caused by destruction of the meta-stable soil structure in loose sandy soil mass, that the failure will occur before stress path reaches the failure line, while, sliding surface liquefaction takes place only along a sliding surface, that need not destruction of the structure. It can take place even in medium or dense soil structure because grain crushing along the sliding surface results in volume shrinkage and pore pressure generation" (Sassa et al., 1996).

A new undrained ring-shear system was used in this study (Sassa, 1997). Besides its advantage of limitless shear displacement, the undrained capability of this system can simulate the stress state along the shear zone of a slide, which is regarded as the undrained condition during landslide motion.

The main purpose of this study is on the sliding surface liquefaction behavior of sandy soil. It aims to verify the relation of grain crushing and high-mobility, and to analyze the excess pore pressure

behavior of different types of soil during sliding surface liquefaction. The susceptibility of sliding surface liquefaction of various samples were analyzed in undrained speed-controlled tests, and, different initial conditions of slopes, different initial relative densities, and frequencies of cyclic-loading were involved in undrained cyclic-loading tests.

2. Setup of the ring-shear system

A new intelligent-type, undrained dynamic-loading ring-shear system was used in this study. This system consists of two sets of apparatus, designated as DPRI-5 (a smaller shear box with 120 mm (inside) and 180 mm (outside) diameters) and DPRI-6 (a larger shear box with 250 mm (inside) and 350 mm (outside) diameters). The shear surface area of shear box for them is 141.37 cm^2, and 470.94 cm^2, respectively. The maximum shear speed at the center of sample is about 10 cm/sec for DPRI-5 and 224 cm/sec for DPRI-6. Frequency of cyclic-loading ranges from 0.01 to 5 Hz. The maximum data-recording rate is 200/sec.

The apparatuses were introduced by Sassa (1997), and Wang and Sassa (1997). The comparison among DPRI-3, 4 (the previous versions), and DPRI-5, 6 was introduced by Vankov and Sassa (1998). In this research, DPRI-5 was used for the undrained cyclic-loading tests (CU-C test), and DPRI-6 was used for the consolidated drained speed-controlled test (CD test) and consolidated undrained speed-controlled test (CU test).

3. Samples properties

Toyoura standard sand (T-sample), silica sand (S-sample) and Osaka group coarse, sandy soil (O-sample) were used in this study.

T-sample is predominantly a uniform subangular to rounded quartz fine sand with approximately 90% of quartz and 4% of chert.

S-sample sand is construction material for industrial use. It is made of weathered silica sand, and has a uniform grain size distribution. The grain is almost angular. It consists of 92 ~ 98% of quartz, and a little amount of feldspar. In this study, the silica sand no.7, with a mean grain size of 0.16 mm was used.

O-sample was taken from the Takarazuka landslide, located in the Takarazuka Golf Club, which was triggered by 1995.1.17 Hyogoken-Nanbu earthquake (Sassa et al., 1996). Osaka group is a limnetic and marine deposits of Pliocene to Mid-Pleistocene distributed around Osaka area (Itihara,
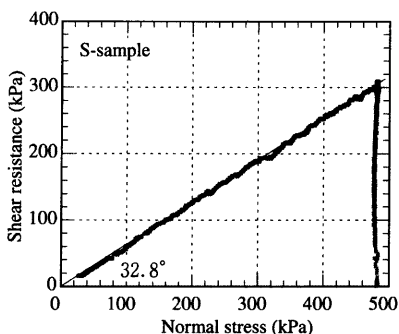
1996). It comes from weathered granite and is composed of 77 percent of quartz and 23 percent of feldspar. The grain is angular. In this study, due to
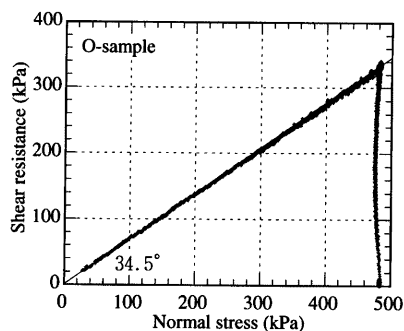
(a) O-sample
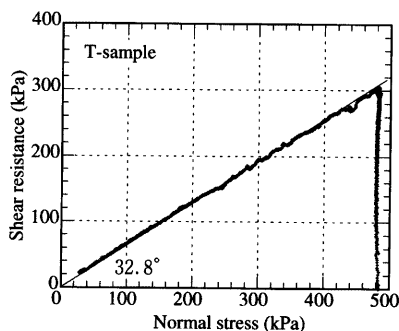
(b) T-sample

(c) S-sample

Fig. 1 Ring-shear test results for residual friction angle on the three samples (shear speed = 3 mm/sec).

Table 1 Calssification property of samples

Classification property	T	S	O
Mean grain size, D_{50} (mm)	0.18	0.16	0.80
Effective grain size, D_{10} (mm)	0.11	0.09	0.28
Coefficient of uniformity, Cu	1.7	2.1	4.7
Maximum void ratio, e_{max}	0.98	1.30	1.17
Minimum void ratio, e_{min}	0.61	0.71	0.66
Specific gravity, Gs	2.64	2.64	2.61
Residual friction angle, ϕ (degree)	32.8	32.8	34.5

Table 2 Relative density of test samples

Test No.	D_{ri} (%)	D_{rc} (%)
T-CD	21.6	39.7
S-CD	40.7	60.8
O-CD(L)	2.94	87.1
O-CD(D)	81.4	100.8
T-CU	25.1	45.9
S-CU	38.8	63.6
O-CU(L)	2.94	93.5
O-CU(D)	81.4	98.0

the needs of apparatuses, grains larger than 4.75 mm were sieved out.

To get the residual friction angle of the three sandy soils, speed-controlled ring-shear tests were conducted with dry sample. The procedure is (1) set oven-dried sample in the ring-shear box; (2) consolidate the sample under 490 kPa; (3) Shear the sample at 3 mm/sec. After the residual strength was reached, during shearing, reduce the normal stress gradually. The obtained failure line and residual friction angle for the three samples were presented in Figure 1. Some classification and index properties of the employed samples are listed in Table 1.

4. Test program

In this study, three series tests were planned. They are: (1) shear speed-controlled drained ring-shear test (CD-test) to investigate grain crushing susceptibility; (2) shear speed-controlled undrained ring-shear test (CU-test) to investigate the excess pore pressure generation behavior; and (3) undrained cyclic-loading ring-shear test (CU-C test), to study the sliding surface liquefaction behavior of sandy soil at cyclic-loading, and analyze the effects of soil type, initial relative density, initial stress state, and frequency of cyclic-loading on high-mobility and excess pore pressure generation.

Natural falling method was used for preparing loose samples (indicated as L for O-sample and no sign for the others), while tamping method was used to make dense samples (indicated as, D).

4.1 Shear speed-controlled ring-shear tests

In this series of tests, CD-test and CU-test were conducted. CD-test was mainly to investigate the grain crushing susceptibility. As by-products, the compression index, Cc for each samples were also obtained. The procedure for CD-test is: (1) set oven-

dried sample in the ring shear box; (2) consolidate the sample under normal stress of $p_1 = 98$ kPa and $p_2 = 196$ kPa, respectively, and calculate the corresponding void ratio, e_1 and e_2. Then, the compression index,

$$Cc = (e_1 - e_2)/ (\log(p_2) - \log(p_1)) \qquad (1)$$

can be obtained; (3) shear the sample at shear speed of 3 mm/sec under normal stress of 196 kPa. (4) after the CD ring-shear test, take the sample in the shear zone and analyze the grain-size distribution.

It needs to mention that, to evaluate the grain crushing susceptibility caused by shearing only, samples of the same relative density with that in CD tests were prepared, and consolidated under normal stress of 196 kPa. Then the consolidated samples were taken out, and grain-size distribution was analyzed.

For CU-test, the procedure is: (1) set oven-dried sample in the ring shear box; (2) saturated the sample through CO_2 and de-aired water (details can be obtained in Wang et al. (1997); (3) consolidate the sample at 50 kPa and confirm the degree of saturation by B_D (= $\Delta u / \Delta \sigma$). B_D value is pore pressure parameter in the direct shear state (Sassa, 1985). A high B_D value indicates a high degree of saturation. The samples with B_D values higher than 0.95 were used in the undrained tests. (4) consolidate the sample at 196 kPa or so, and shear it at constant speed of 3 mm/sec.

Basically, final shear displacement for both CD-tests and CU-tests was 42 m. However, in CU-test, test was closed early when the pore pressure could not generate any more.

The test parameters are listed in Table 2. D_{ri} is the initial relative density of a sample before application of any load, while D_{rc} is relative density after normal consolidation.

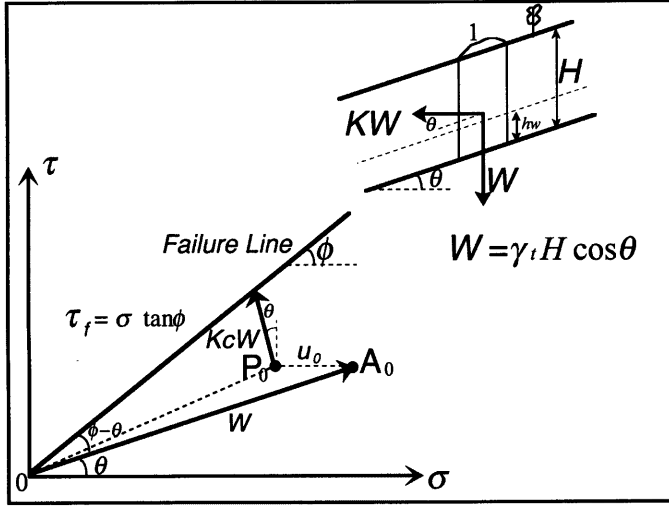$$W = \gamma_t H \cos\theta$$

$$\tau_f = \sigma \tan\phi$$

Fig. 2 Schematic diagram of the undrained cyclic-loading ring-shear tests.
A_0: Initial stress state in dry condition. $\sigma_0 = W\cos\theta$, $\tau_0 = W\sin\theta$;
P_0: Initial stress state when initial pore pressure $u_0 = \gamma_w h_w \cos^2\theta$ exists.

4.2 Undrained cyclic-loading ring-shear tests

This consolidated-undrained cyclic-loading test (CU-C test) simulates the stress condition of a soil element subjected to a horizontal seismic force in the sliding zone of an infinitely long slope (Figure 2). To represent an "ideal" slope, depth of potential sliding surface was assumed to be 30 m, slope angle to be 25° , and initial pore pressure $u_0 = 20$ kPa. $\gamma_t = 20$ k N / m³ was taken as the unit weight of all the samples. A condition of 15° of slope angle was also considered to analyze the effect of initial stress state, as well as a test with dense O-sample was planned to analyze the effect of initial relative density on the "Sliding surface liquefaction". The seismic coefficient ratio, K/Kc is defined as the cyclic stress amplitude parameter. Where, K is horizontal seismic coefficient, and Kc is the critical seismic coefficient for the stress path to reach the failure line by adding KcW to the initial stress point P_0 in Figure 2. Kc can be given by Eq. (2) .

$$Kc = \tan(\phi - \theta) - [\tan\theta + \tan(\phi - \theta)]u_0\sin\theta/W \quad (2)$$

Where, ϕ is the angle of residual friction of sample (in Fig. 1). Thus, the critical increment of normal stress and shear stress causing slope to fail can be calculated as:

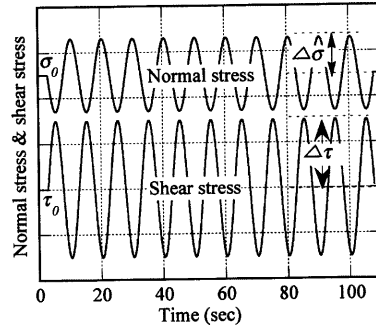$$\triangle\sigma_c = Kc\ W\ \sin\theta \quad (3)$$

Fig. 3 Stress pattern used in the undrained cyclic-loading ring-shear tests (case of frequency = 0.1 Hz).

$$\triangle\tau_c = Kc\ W\cos\theta \quad (4)$$

To study the post-failure behavior of soils, $K/Kc = 1.5$ was used for all of the tests, while $K/Kc = 2.0$ was used for a dense O-sample test. The amplitude of normal stress increment:

$$\triangle\sigma = K/Kc\ \triangle\sigma_c \quad (5)$$

and shear stress increment:

Table 3 Sample relative densities and amplitude of cyclic-loading.

Test No.	D_{ri}	D_{rc}	Kc	$\Delta\sigma$	$\Delta\tau$
T-C(0.1)-25°	32.7	43.2	0.128	48.5	104.1
S-C(0.1)-25°	51.6	67.8	0.128	48.5	104.1
O-C(0.1)-25°	22.8	111.1	0.157	59.7	128.1
O-C(0.5)-25°	22.8	117.6	0.157	59.7	128.1
O-C(0.02)-25°	22.8	115.4	0.157	59.7	128.1
O-C(0.1)-15°	22.8	115.8	0.348	76.7	286.3
O(Dense)-C(0.1)-25°($K/Kc = 1.5$)	111.2	119.8	0.157	59.7	128.1
O(Dense)-C(0.1)-25°($K/Kc = 2.0$)	111.2	119.8	0.157	79.6	170.8

$$\Delta\tau = K/Kc \, \Delta\tau_c \qquad (6)$$

Fig. 4 Variation of sample height during speed-controlled drained ring-shear tests.

The relative density of sample (at initial state and after consolidation) and amplitude of cyclic-loading is listed in Table 3.

Cyclic loads of constant amplitude lasted for 10 cycles with different frequencies of 0.02 Hz, 0.1 Hz, and 0.5 Hz were loaded after the initial stress and pore pressure were applied (Figure 3). The CU-C test was named in the order of soil name-cyclic-loading (frequency)-slope angle, except the test on dense O-sample. For example, O-C(0.1)-25° means that the sample is O-sample, frequency of cyclic-loading is 0.1 Hz, and the angle of the ideal slope is 25°.

5. Consolidated-drained (CD) ring-shear test results

At first, the CD tests were performed. Variation of sample height versus shear displacement is presented in Figure 4. In compression (shrinkage), sample height is decreased, while in dilatancy, sample height is increased. All of the curves show that, at the onset of shear (until 7.0 mm), the samples were compressed; from 7.0 mm to 25 mm, O-CD(D), showed a dilative tendency, S-CD and T-CD seem to be no volume change, and compression rate in O-CD(L) turned smaller. Thereafter, samples shrank with the shear displacement at different rates. The rates for O-CD(L) and O-CD(D) are about the same, and for S-CD and T-CD, they are almost the same but smaller. The shrinkage speeds of O-sample at loose and dense states are obviously larger than that of S-sample and T-sample.

After drained shear tests were over, it was observed that, except T-CD, grain crushing mainly generated in the shear zone of 10 ~ 20 mm. Figure 5
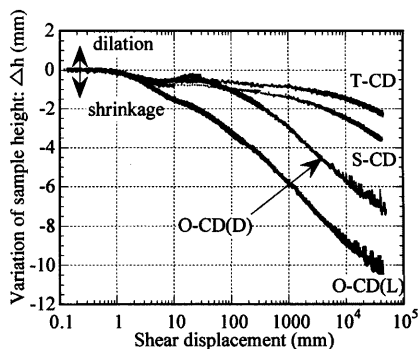
is the results of the grain-size distribution analysis of samples after consolidation and samples taken from shear zone after shearing. For simplification, Marsal's breakage factor, B, is used to quantify the grain crushing susceptibility (Marsal, 1967). This method involves the change in individual particle sizes between the initial and final grain-size distribution. The difference in the percentage retained is computed for each sieve size. This difference will be either positive or negative. Marsal's breakage factor, B, is the sum of the differences having the same sign. The B value for T-CD was 0.2%, for S-CD was 3.4 %, for O-CD(L) was 8.2%, and for O-CD(D) was 9.0%. The Marsal's breakage factors, B, as well as the compression index, Cc of samples at a certain relative density, against the final sample height changes, are plotted in Figure 6. It is indicated a good relationship between the sample height change and the grain breakage factor, B, and the compression index, Cc. When $B = 0$, the final sample height change is -2.0 mm. It presented that volume shrank even with little or no grain crushing. The motion of fine grain to the pore in the coarse grain skeleton could due mainly cause the phenomenon. From Fig. 6, it is found that, at drained condition, the variation of sample during shearing is determined by two factors: grain crushing and compression, and the variation of sample height consists of two parts: one part is caused by grain crushing, one is caused by the rearrangement of the grains as mentioned above. Because the sample height change has a near lineal relation with grain breakage factor, B, the variation of sample height could be used as a relative index to evaluate the grain crushing susceptibility.

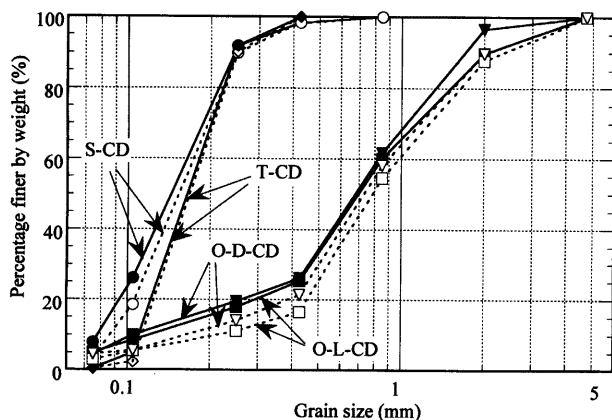There are many papers concerning with grain crushing (Fukuoka, 1991; Lade et al., 1996).

Fig. 5 Grain-size distribution of samples after consolidation and samples taken from the shear zone after shear finished. Dotted line: sample after consolidation; Solid line: sample from the shear zone after sheared.

According to the above test results, it is found that the internal affecting factors on grain crushing are 1) Mineral component. Sands consisting of hard minerals such as quartz are difficult to be subjected to the grain crushing than those consisting of feldspar and mica. 2) Grain shape. Sands with angular shape are easier to be crushed than those with rounded grains. S-sample and T-sample are mainly composed of quartz, but S-sample was easily crushed. It is probably because S-sample is angular, while T-sample is rounded.

6. Consolidated-undrained (CU) ring-shear test results

The initial relative densities of samples in CU tests were about the same with CD tests as shown in Table 2. In Figures 7, the excess pore pressure ratios during tests are presented. Effective stress paths for all four tests are shown in Figures 8. Excess pore pressure ratio is expressed as the ratio of excess pore pressure increment to initial effective normal stress (Popescu et al.,1997). If evaluating the high mobility of post-failure behavior of soils by the excess pore pressure ratio greater than 0.7, high mobility was observed in O-CU(L), O-CU(D) and S-CU. However, the case of S-CU showed high excess pore pressure ratio (>0.7) after long shear displacement of 2000 mm. Because real situation is not a completely undrained condition, there will be considerable pore pressure dissipation took place during the long shear displacement, therefore, silica sand (S-sample) will
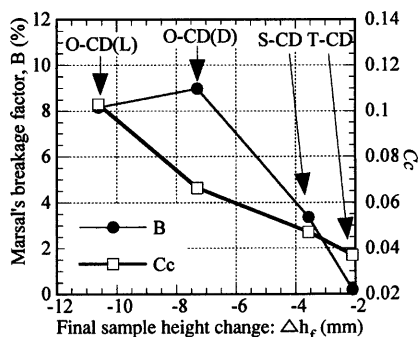

Fig. 6 The relationship between final sample height change and Marsal's breakage factor, B, and compression index, Cc.

unlikely cause high mobility. During the undrained shearing, T-sample had large pore pressure dissipation from 3.0 mm to 150 mm of shear displacement, and had less pore pressure generation during long shear displacement, it is not a soil showing high-mobility.

The characteristics of sliding surface liquefaction and (mass) liquefaction can be observed in Figures 8. In test O-CU(L) (Fig. 8(a)), because of loose structure, the soil failed before the stress path reached the failure line at first, formed a stress path of (mass) liquefaction. Thereafter, the stress level reduced along the failure line when shear

displacement increased. In test O-CU(D) (Fig. 8(b)), the stress path once reached the failure line, then, it went upward along the failure line because of high density and the resulting dilatancy. However, the stress path went downward along the failure line until a very small stress with shear displacement increasing thereafter. The high pore pressure generation with the progress of shear displacement is caused by grain crushing in the shear zone (Sassa, 1996; Sassa et al., 1996). This is a typical stress path of the sliding surface liquefaction. T-sample showed almost no stress reduction after sheared for 42 m (Fig. 8(c)). Stress path of test on S-sample in Fig. 8(d) showed a medium behavior between O-CU(L) and T-CU. It indicates that: at loose and dense state, O-sample is susceptible to generate high-mobility (either in liquefaction type, or in sliding surface liquefaction type), S-sample can generated high excess pore pressure after very long shear displacement in the "ideal" undrained condition, while T-sample can not show high-mobility.

Comparing the results of CU and CD tests, it is easily found that, the process of pore pressure generation with shear displacement in CU test, is similar to that of the sample height change process with shear displacement in CD test. Both of the

processes are mainly controlled by grain crushing (although the compression property and grain rearrangment also has some effects on it). So, the susceptibility of high mobility phenomenon of sandy soils can be estimated by the sample height change behavior in drained ring shear tests. This makes
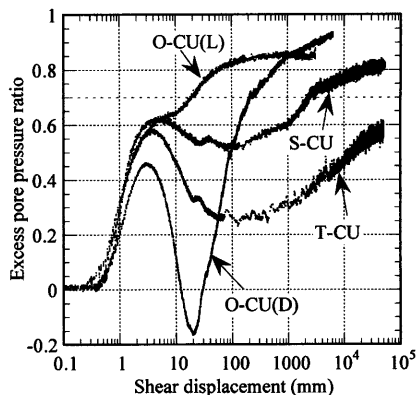

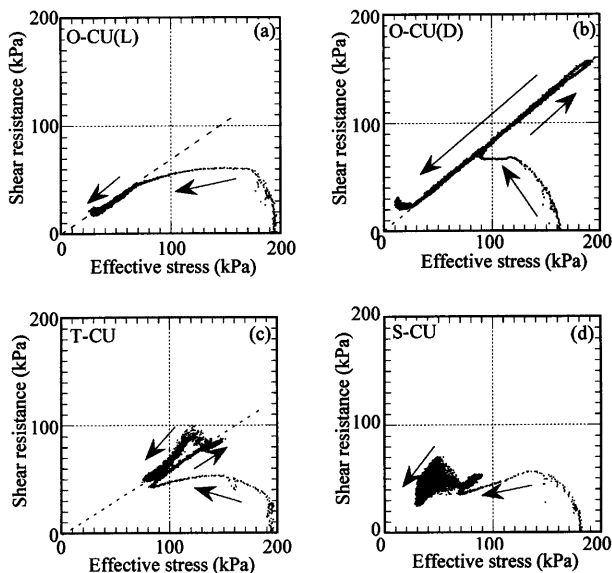Fig. 7 Excess pore pressure ratio of various samples in speed-controlled CU tests.

Fig. 8 Laboratory-determined stress path of various samples in speed-controlled CU tests.
Shear speed = 3 mm/sec. (a) Loose O-sample, (b) Dense O-sample, (c) T-sample, (d) S-sample.

possible the prediction of high mobility behavior of failures even by means of drained ring shear test which can be done by the conventional ring shear apparatus (Bishop et al., 1971) or even by drained shear test with shear box.

7. The undrained cyclic-loading (CU-C) ring-shear test results

In consolidated undrained cyclic-loading (CU-C) ring-shear tests, after confirmation of B_D value, the sample was normally consolidated. Only those samples with B_D value higher than 0.95 were tested continually. Then, both initial pore pressure and initial shear resistance were applied in the drained condition. Finally, normal stress increment ($\triangle \sigma$) and shear stress increment ($\triangle \tau$) were applied simultaneously under the undrained conditions.

7.1 Description of CU-C tests

All of the time-series data and stress path (total stress path (TSP) and effective stress path (ESP) is concluded) of the CU-C tests are presented. From the time-series data, the change of pore pressure, shear resistance, and shear displacement, can be checked. While, in the stress path, whether the tested sample generated high mobility or sliding surface liquefaction, can be determined. The apparent friction angle ϕ_a, defined as (Lee et al., 1996):

$$\tan \phi_a = (\text{Final shear resistance}) / (\text{The initial total stress}) \qquad (7)$$

can be calculated and used as an evaluation index of soil mobility.

(1) Test O-C(0.1)-25°

Fig. 9 shows the test results of O-C(0.1)-25°. The O-sample used in the test was at loose state. From the time-series data, it is found that, at the first cycle, the sample failed, because the shear resistance did not increase up as the shear stress was applied. At the same time of the failure of sample, pore pressure generated rapidly. At the beginning of the second cycle, the pore pressure reached its peak value, and shear resistance decreased to a small value. Thereafter, shear resistance kept the constant value, while pore pressure varied at the same phase with the cyclic-loading of normal stress. Only the shear displacement increased. The state of the sand deforming continually, at constant volume and under constant shear stress and normal stress, is called 'steady state' (Castro, 1975). From the stress path, it is found that, from the start point, the effective stress

path (ESP) reached the peak failure line, and the stress reduced along the failure line. In this process, the failure line shows a change from peak failure line to residual failure line. From the total stress path, it can be checked that, at the end of the second cycle of cyclic-loading, the shear resistance became to the constant value. It is obviously, high-mobility phenomenon generated in this test. Because the ESP line reduced along the failure line. It is recognized that the sliding surface liquefaction generated. The final apparent friction angle is only 3.6°.

(2) Test T-C(0.1)-25°

The test results of test T-C(0.1)-25° were shown in Figure 10. They are very different from those in test O-C(0.1)-25°. In the time-series data, it can be checked that the sample also failed in the first cycle, because the upper phase of shear resistance did not raise to the peak as that applied in shear stress. But in the whole process, the shear resistance showed a decreasing trend, pore pressure showed an increasing trend, and shear displacement increased cycle by cycle gradually. At the end of ten cycles of the cyclic-loading, the final shear displacement was only about 360 mm. Shear displacement ceased at the end of cyclic-loading.

In the stress path, from the start, the ESP line reached failure line, and showed a bit decrease along the failure line. However, the shear resistance at the end of cyclic-loading, is larger than the initial shear stress. The high-mobility phenomenon did not generate in this test.

(3) Test S-C(0.1)-25°

Figure 11 shows the test results of S-C(0.1)-25°. The shear resistance in the time-series data shows a gradual decreasing tendency, and pore pressure increased cycle by cycle. The generation of pore pressure is slower than that in test O-C(0.1)-25°. The ESP shows the stress reduced along the failure line, but at the end of cyclic-loading, the stress level is not so small. The apparent friction angle is 12.9°. Somewhat mobility generated in this test, but the high-mobility was not reached.

(4) Test O-C(0.02)-25°

This test is to analyze the effect of frequency of cyclic-loading on the sliding surface liquefaction. The frequency is 0.02 Hz. Time-series data and stress path is shown in Figure 12. At the first cycle, the pore pressure reached its peak value, and shear resistance reduced to the constant low value. Thereafter, typical characteristic of "steady state" can be observed. The apparent friction angle at the end of cyclic-loading is 2.9°. Because cyclic-loading with lower frequency has larger energy, or Arias intensity (Kayen et al., 1997). The Arias intensity measure (also termed

Fig. 10 Time-series data (upper) and stress path (lower) of T-C(0.1)-25°
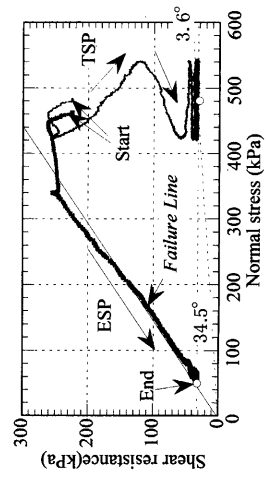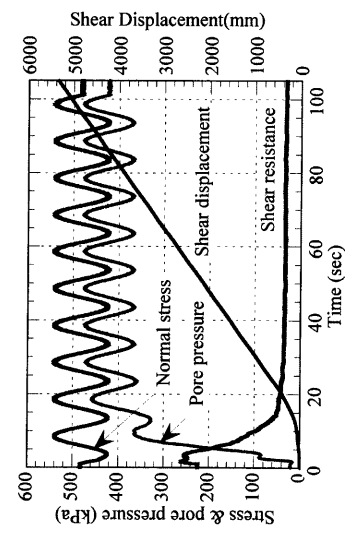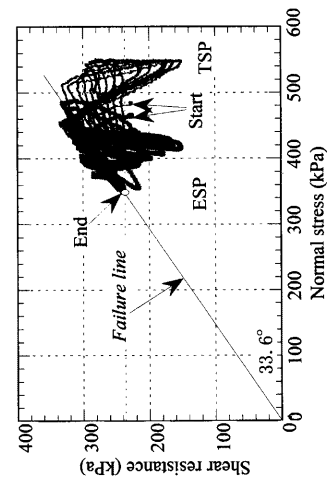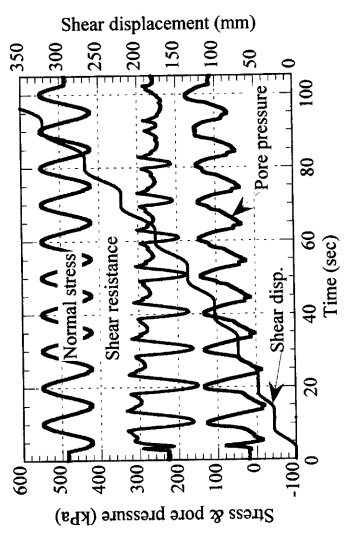TSP: Total stress path; ESP: Effective stress path.

Fig. 9 Time-series data (upper) and stress path (lower) of O-C(0.1)-25°
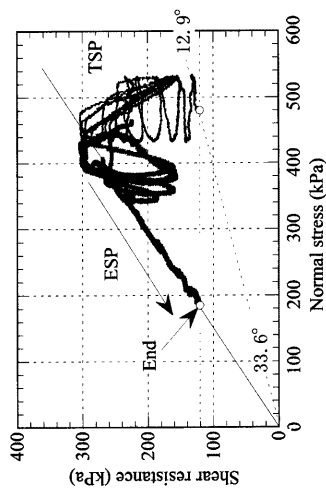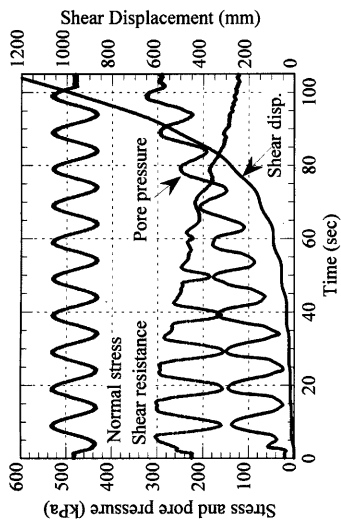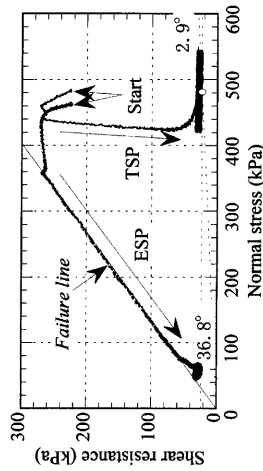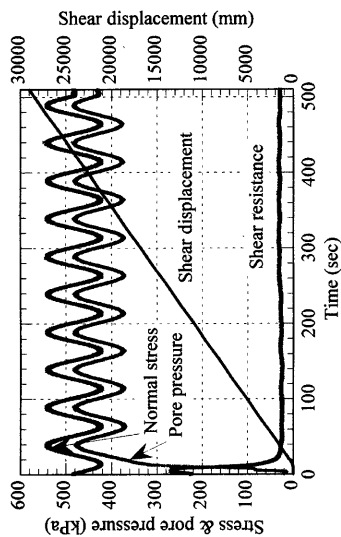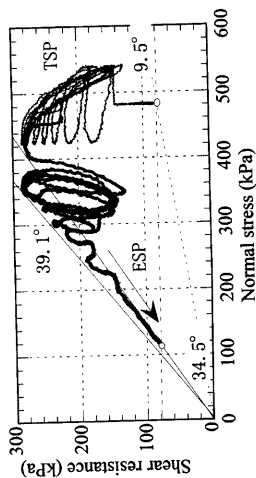TSP: Total stress path; ESP: Effective stress path.

Shear displacement (mm)

Shear displacement

Shear resistance

Normal stress

Pore pressure

Time (sec)

Stress & pore pressure (kPa)

Failure line

ESP

TSP

Start

2.9°

36.8°

Shear resistance (kPa)

Normal stress (kPa)

Fig. 12 Time-series data (upper) and stress path (lower) of O-C(0.02)-25°. TSP: Total stress path; ESP: Effective stress path.

Shear Displacement (mm)

Pore pressure

Shear disp.

Normal stress

Shear resistance

Time (sec)

Stress and pore pressure (kPa)

TSP

ESP

End

12.9°

33.6°

Shear resistance (kPa)

Normal stress (kPa)

Fig. 11 Time-series data (upper) and stress path (lower) of S-C(0.1)-25°. TSP: Total stress path; ESP: Effective stress path.
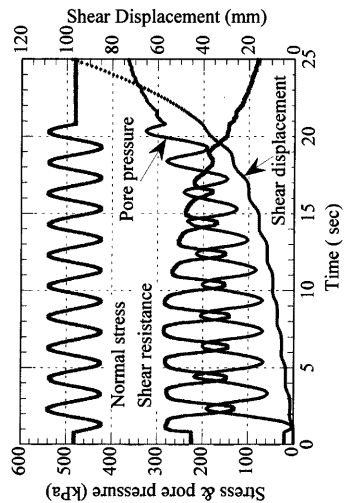
Fig. 13 Time-series data (upper) and stress path (lower) of O-C(0.5)-25° .
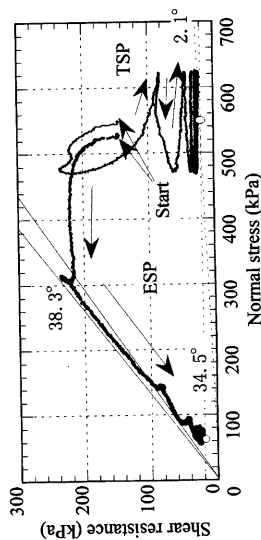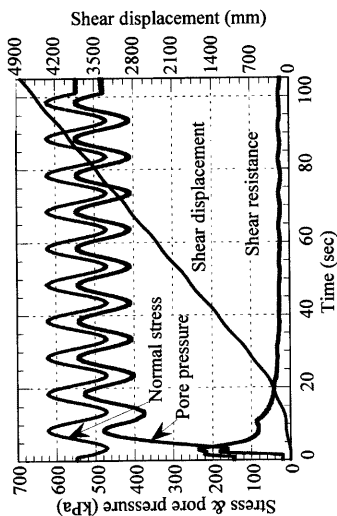TSP: Total stress path; ESP: Effective stress path.

Fig. 14 Time-series data (upper) and stress path (lower) of O-C(0.1)-15°
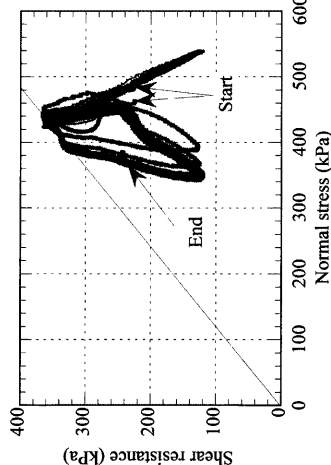TSP: Total stress path; ESP: Effective stress path.

Fig. 16 Time-series data (upper) and stress path (lower) of O(Dense)-C(0.1)-25° at K/Kc = 2.0. TSP: Total stress path; ESP: Effective stress path
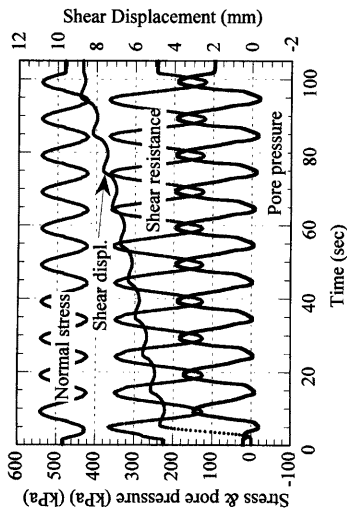

Fig. 15 Time-series data (upper) and stress path (lower) of O(Dense)-C(0.1)-25° at K/Kc = 1.5. TSP: Total stress path; ESP: Effective stress path.
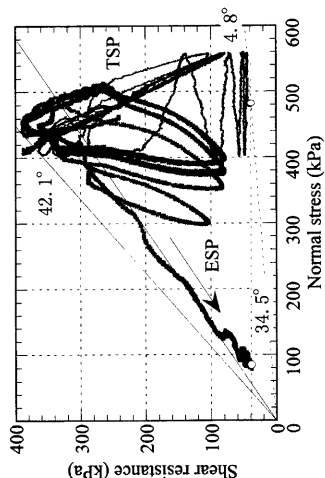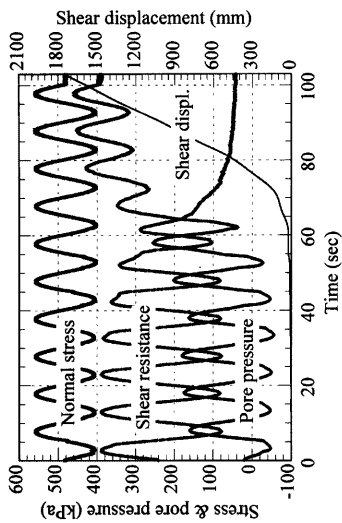
accelerogram energy) is the sum of the energy absorbed by a population of simple osillators evenly in frequency (Arias, 1970). It is certain that cyclic-loading with lower frequency would make high-mobility generation easier.

(5) Test O-C(0.5)-25°

This test is one of the series tests to analyze the effect of frequency on sliding surface liquefaction. The frequency is 0.5 Hz. It has smaller energy than that in test O-C(0.1)-25° and O-C(0.02)-25°. From the time-series data and stress path presented in Figure 13, it is easily found that, the reduction of shear resistance and generation of pore pressure is slower. After the ten cycles of cyclic-loading finished, the pore pressure also generated. The apparent friction angle at the end of cyclic-loading is 9.5°.

(6) Test O-C(0.1)-15°

This test is to analyze the effect of initial stress state on the sliding surface liquefaction, because there were so many landslide occurred on gentle slopes (Zhang, 1996). Figure 14 shows the test results. Comparing them with test results of O-C(0.1)-25°, a similar pattern could be found. However, at the end of cyclic-loading, the shear displacement is about 4800 mm, and the apparent friction angle is 2.1°. It is smaller than that in test O-C(0.1)-15°. It is concluded that at the same K/Kc value, gentle landslide generate high-mobility easily.

(7) Tests on dense O-samples

A test on dense O-sample at the same dynamic condition with that in test O-C(0.1)-25° was planned to analyze the effect of initial relative density on the sliding surface liquefaction. According to Sassa et al. (1996), sliding surface liquefaction can generate even in medium and dense sandy soil, while (mass) liquefaction can only generate in loose sandy soil. The test results at $K/Kc = 1.5$ were shown in Figure 15. At the end of cyclic-loading, the shear displacement was only 8.6 mm, and the excess pore pressure was just 80 kPa. From the stress path, it is difficult to justify whether the sample failed. Because the Kc value was obtained based on residual friction angle, but dense sample would have high peak strength, the cyclic stress intensity may be too small to cause the dense sample fail.

So, a test on dense O-sample at $K/Kc = 2.0$ was carried out. The test results were presented in Figure 16. In the time-series data, shear resistance reduced greatly after the seventh cycle. Thereafter, the shear displacement generated rapidly, while pore pressure reached the peak value at the eighth cycle. The stress path shows that, the first seven cycles of cyclic-loading make the sample reach its peak strength (peak friction angle = 42.1°). After the residual strength was reached, the ESP reduced to the constant value. At the last two cycles, the sample reached the steady state. The apparent friction angle is 4.8°. It is obviously that the high-mobility generated, with a typical effective stress path of sliding surface liquefaction.

7.2 Excess pore pressure and shear displacement

In the time-series data described above, it is found that, after the sample reached the steady state, pore pressure varied at the same phase with normal stress, and large pore pressure always generates when large shear displacement generates. According to Sekiuchi et al. (1998), under the undrained cyclic-loading, the measured pore pressure can be divided into two components: fluctuating component and residual component. The fluctuating component is mainly caused by variation of normal stress increment. It is almost equal to the increment of normal stress under fully saturated condition. The residual component is mainly due to plastic shear displacement. As an example, Figure 17 shows the data-processing with test result of O-C(0.1)-25°. The residual component was refined from the total pore pressure for these series tests to show the generation of excess pore pressure with shear displacement.

(1) Results of various samples in CU-C tests

To show the difference excess pore pressure generation behavior induced by samples themselves, the excess pore pressure generated in test O-C(0.1)-25°, T-C(0.1)-25°, and S-C(0.1)-25°, the CU-C tests on O-sample, T-sample and S-sample at $K/Kc = 1.5$ with cyclic frequency = 0.1 Hz, are presented in Figure 18.

The results show the same trend as that observed in the speed-controlled CU tests. If also evaluating high mobility by pore pressure greater than 0.7, O-C(0.1)-25° shows high mobility, while T-C(0.1)-25° did not show high-mobility. S-C(0.1)-25° shows a trend similar to O-C(0.1)-25°, but the rate of pore pressure generation is smaller. The pattern of pore pressure generation with shear displacement is almost the same as that in the speed-controlled CU tests.

It is indicated that, in cyclic-loading, grain crushing also strongly affected the excess pore pressure behavior of sandy soils.

(2) Results of O-samples at various frequencies

Frequency is an important index of seismic wave. To investigate how the frequency affects the pore pressure behavior under the undrained
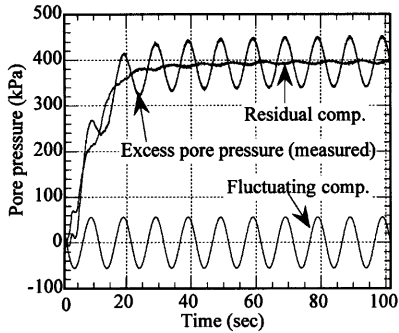
Fig. 17 Composing components of pore pressure ratio in CU-C tests (with the data of O-C(0.1)-25°).
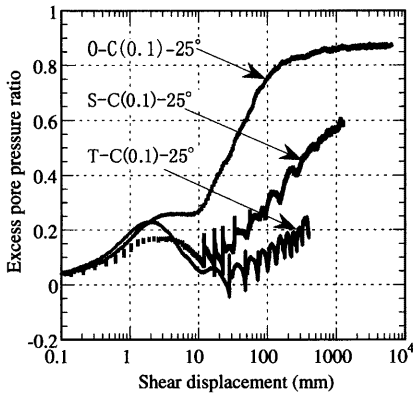

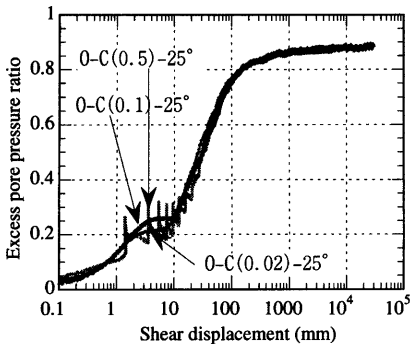Fig. 18 The residual excess pore pressure ratio of various samples in CU-C tests.

Fig. 19 The residual pore pressure ratios of O-samples in CU-C tests with different frequencies.

condition, two frequencies of 0.02 Hz and 0.5 Hz were used in the CU-C tests on O-sample. The results were compared with that of O-C(0.1)-25 and shown in Figure 19. O-sample generated high mobility at 100 mm of shear displacement for all tests. Before that, although test data with 0.5 Hz can not be clarified because of noise, the excess pore pressure ratio of 0.1 Hz is larger than that of 0.02. There are two possible reasons for this phenomenon. (1) For the same shear displacement, greater number of cycles is loaded in the higher frequency. Pore pressure generation may be affected by the cycle number of cyclic-loading; (2) Higher frequency causes faster pore pressure generation. Faster pore pressure generation will effectively build up excess pore pressure in the shear zone, because excess pore pressure will dissipate upwards and downwards from the shear zone in the shear box.
(3) Results of O-samples in various initial stress states

This is to compare the pore pressure behavior of O-sample at different slope angle of 15° and 25° . Figure 20, is the test results of O-C(0.1)-25° and O-C(0.1)-15° . Under the same value of K/Kc (= 1.5), the excess pore pressure responses of O-sample, can be compared. Both curves show a slight decrease or at least no increase from 4.0 mm to 10 mm shear displacement. With the same mechanism as that in speed-controlled CU tests, this is caused by the dilative behavior when the soils begin to be sheared. Thereafter, the pore pressure ratio increased rapidly as the shear displacement increased, and then caused high-mobility. The difference is that the pore pressure response is higher in 15° slope than that in 25° slope. It is indicated that, under the same K/Kc condition, high-mobility phenomenon takes place easier in gentler slope. This is because that, when K/Kc values are kept the same, the shear stress increment acts in the gentler slope is larger than that acts in the steeper one.
(4) Results of O-sample at different initial relative densities

Figure 21 shows the comparison of loose O-sample at K/Kc = 1.5, 0.1 Hz and dense O-sample at K/Kc = 2, 0.1 Hz. The loose sample almost had no pore pressure dissipation in the whole shearing process. It went to high-mobility directly. While, dense O-sample, generated negative excess pore pressure before 10 mm of shear displacement, this is caused by dilatancy resulting from the initial dense state. Thereafter, the excess pore pressure generated rapidly from 10 mm to 100 mm of shear displacement. This phenomenon is similar to that in the speed-controlled CU tests. It is indicated that, on
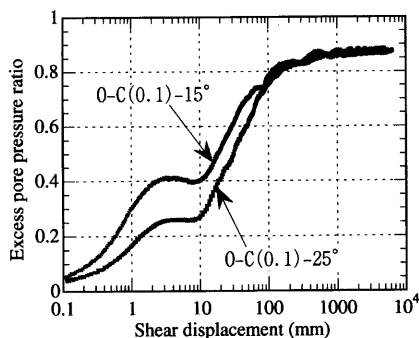
Fig. 20 The residual pore pressure ratios of O-samples in CU-C tests at different initial slope angles.

Fig. 21 The residual excess pore pressure ratio of O-samples in CU-C tests at loose and dense state.

the soils susceptible to grain crushing, sliding surface liquefaction could generate even in dense state.

8. Conclusion

The following conclusion may be drawn from the results obtained in the ring-shear tests with different sands and sandy soils.

Grain crushing can be evaluated with the variation of sample height in the CD ring-shear test for a certain shear displacement. The variation of sample height provides a good relationship with the grain breakage factor, *B*.

The sliding surface liquefaction behavior in CU tests can be estimated by the results of CD tests. The soils susceptible to grain crushing are prone to the sliding surface liquefaction in the saturated undrained condition.

The excess pore pressure generation in the CU-C tests on various samples show the same trend with that in speed-controlled CU tests. The excess pore pressure behavior obviously depends on the grain crushing characters during shearing.

At different initial slope angles for a soil, the high-mobility generated easier at the gentler slope.

For different frequency, it is shown that higher frequency causes excess pore pressure generate more quickly.

Sliding surface liquefaction can generated in soils susceptible to grain crushing, even at dense state.

Acknowledgements

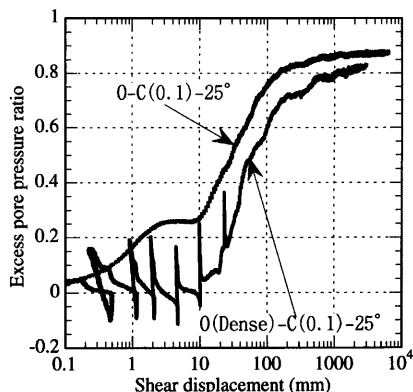The writers wish to thank Associate Professor

References

Arias, A. (1970): A measure of earthquake intensity. R. J. Hansen, ed. *Seismic Design for nuclear Plants*. MIT Press, Cambridge, Mass, pp.438-483.

Bishop, A. W., G. E. Green, V. K. Garga, A. Andresen and Brown J. D. (1971): A new ring shear apparatus and its application to the measurement of residual strength, *Geotechnique*, Vol. 21, No. 4, pp. 273-328.

Castro, G. (1969): *Liquefaction of Sands*. Harvard University, Cambridge, Harvard Soil Mechanics Series, No. 81, pp. 1-80.

Castro, G. (1975): Liquefaction and cyclic loading of saturated sands. *J. Geotech. Engineering*, Div. ASCE, Vol. 101, No. GT6, pp. 551-569.

Fukuoka, H. (1991): Variation of the friction angle of granular materials in the high-speed high-stress ring shear apparatus, -Influence of re-orientation, alignment and crushing of grains during shear-, *Bulletin of Disaster Prevention Research Institute, Kyoto University*, Vol. 41, No. 4, pp. 243-279.

Ishihara, K. (1993): Liquefaction and flow failure during earthquakes. *Geotechnique*, Vol. 43, No. 3, pp. 351-415.

Itihara, M. (1996): *The Osaka group layer and Chinese loess layer* (in Japanese). Tokyo: Chikuji-Shokan, pp. 12-85.

Kayen, R. E. and Mitchell, J. K. (1997): Assessment

of liquefaction potential during earthquakes by Arias intensity. *J. Geotech. and Geoenvironmental Engineering*, Vol. 123, No. 12, pp. 1162-1174.

Lade P. V., Yamamura J. A. and Bopp P. A. (1996): Significance of particle crushing in granular materials. *J. Geotechnical Engineering*, Vol. 122, No. 4, pp. 309-316.

Lee, J. and Sassa, K. (1996): A study on the apparent friction angle mobilized during the undrained loading in long run-out landslides, *Bulletin of the Disaster Prevention Research Institute*, Kyoto University, Vol. 45, No. 4, pp. 99-124.

Marsal, R. J. (1967): Large scale testing of rockfill materials. *J. Soil Mechanics and Foundations*, Div., ASCE, Vol. 93, No. SM2, pp. 27-43.

Popescu, R., Prevost, J. H. and Deodatis, G. (1997): Effects of spatial variability on liquefaction: some design recommendations. *Geotechnique*. Vol. 47, No. 5, pp. 1019-1036.

Sassa, K. (1985): The mechanism of debris flows. *Proc. of XI Int'l Conference on Soil Mechanics and Foundation Engineering*, San Francisco, Vol. 3, pp. 1173-1176.

Sassa, K. (1996): Prediction of earthquake induced landslides. *Proc. of 7th Int'l Symposium on Landslides*, Rotterdam: Balkema, Vol. 1, pp. 115-132.

Sassa, K., Fukuoka H., Scarascia-Mugnozza G. and Evans S. (1996): Earthquake induced landslides. *Soils and Foundations*, Special Issue, pp. 53-64.

Sassa, K. (1997): A new intelligent type dynamic loading ring shear apparatus. *Landslide News*. No. 10, pp. 33.

Sassa, K., Fukuoka, H. and Wang F. W. (1997): Mechanism and risk assessment of landslide-triggered-debris flows: Lesson from the 1996.12.6 *Otari debris flow disaster, Nagano, Japan. Proc. of the int'l Workshop on Landslide Risk Assessment*, Rotterdam: Balkema, pp. 347-356.

Seed, H. B. and Lee K. L. (1966): Liquefaction of saturated sands during cyclic loading. *J. Soil Mechanics and Foundations*, Div., ASCE, Vol. 92, No. SM3, pp. 83-108.

Sekiuchi, H., Kita, K., Sassa, S. and Shimamura T. (1998): Generation of progressive fluid waves in a geo-centrifuge. *Geotech. Testing J.*, ASTM (in press).

Terzaghi, K. and Peck R. B. (1948): *Soil mechanics in engineering practice*. 2nd edn, Chichester: Wiley, pp. 108-115.

Vankov, D. A. and Sassa K. (1998): Dynamic testing of soils by the ring-shear apparatus. *Proc. of 8th Int'l. IAEG Congress*, Rotterdam: Balkema (in press).

Wang, F. W. and Sassa K. (1997): Shear displacement behavior of sandy soils in different states of saturation and the seismic coefficient in cyclic-loading ring-shear tests. *J. Natural Disaster Science*, Vol. 19, No. 1 (in press).

Zhang, D. (1996): A study on the mechanism of loess landslides induced by earthquakes. *J. Natural Disaster Science*, Vol. 18, No. 1, pp. 27-41.

要　旨

　すべり面液状化現象は砂質土地すべり高速運動の原因の一つとなる。佐々らは「すべり面液状化現象」，すなわち非排水条件下でのせん断ゾーンにおける粒子破砕に伴う過剰間隙水圧の発生によるせん断抵抗が低下するというメカニズムを提案した。本研究では，リングせん断試験機を用いて，三種類の砂質試料について，a) 定圧定速度排水せん断試験, b) 定圧定速度非排水せん断試験, および, c) 設定した斜面条件での一定振幅の繰り返し載荷試験を行い，砂質土斜面のすべり面液状化の発生過程，特に粒子破砕の起こり易さと過剰間隙水圧比の関係を調べた。その結果，以下の結論が得られた：(1) 砂質土のすべり面液状化現象は土粒子破砕の起こり易さと密接な関係がある。粒子破砕の起こりやすい材料ほどすべり面液状化を起こし易い；(2) 砂質土のすべり面液状化の指標となる過剰間隙水圧比は，速度制御や繰り返し載荷に関わらず，試料の特性とせん断距離に関連する；(3) 砂質土のすべり面液状化の発生は排水せん断試験中の沈下量より推定できる；(4) 繰り返し載荷の周波数，初期応力状態、及び初期密度は過剰間隙水圧の発生に影響する。

キーワード：すべり面液状化, リングせん断試験, 地すべり, 繰り返し載荷, 過剰間隙水圧比, 流動化